Lab on a Chip

Devices and applications at the micro- and nanoscale

Accepted Manuscript

This article can be cited before page numbers have been issued, to do this please use: X. Xie, Q. L. Wang, R. Shi, T. Lei, C. ". Kim and M. Wong, *Lab Chip*, 2026, DOI: 10.1039/D5LC00992H.

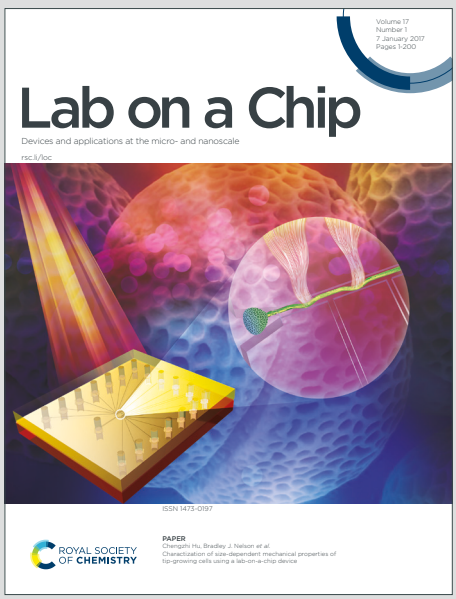

ROYAL SOCIETY OF CHEMISTRY

rsc.li/loc

View Article Online
DOI: 10.1039/D5LC00992H

ARTICLE

Active-Matrix Digital Microfluidic Device Based on Surfactant-Mediated Electro-Dewetting

Xinying Xie, *[a] Qining Leo Wang, [b] Runxiao Shi, [a] Tengteng Lei, *[a] Chang-Jin "CJ" Kim, [b] and Man Wong [a]

Received 00th October 2025,
Accepted 00th January 20xx

DOI: 10.1039/x0xx00000x

Based on electro-wetting mechanism, digital microfluidics (DMF) utilizes both direct-drive and active-matrix (AM) control of electrodes. Recently, DMF with surfactant-mediated electro-dewetting that electrically induces hydrophobic repulsion of droplets containing ionic surfactant has also been demonstrated. However, the existing electro-dewetting DMF devices are on a direct-drive controlled electrode array, which limits the number of independent electrodes. Reported in this work is an electro-dewetting DMF device on an AM array by providing the continuous current needed for electro-dewetting. Indium-tin-zinc oxide top-gate self-aligned thin-film transistors are employed in the cell circuit to address and drive droplets with low voltage. The resulting AM electro-dewetting DMF devices are confirmed to transport, split, and merge droplets by using low voltage, opening the path for electro-dewetting DMF that offers a large number of independent electrodes.

Introduction

Microfluidics can be beneficially applied in life sciences (1-6), chemical synthesis (7, 8), biological and chemical dynamic processes (9, 10), and thermodynamic issues (11-13). It involves the manipulation of fluids in microscale environments and can be categorized into continuous flow-based and droplet-based microfluidics. As a subset of droplet-based microfluidics, digital microfluidics (DMF) manipulates discrete droplets individually and independently (14-17). With unique reconfigurability, DMF facilitates the miniaturization and automation of diverse molecular biology and chemistry experiments, leading to significant reductions in both time and reagent costs (16, 17).

Currently, most DMF systems are realized with electro-wetting-on-dielectric (EWOD) devices (18, 19), where a droplet is electrically attracted onto a hydrophobically coated surface with an apparent decrease of contact angle (18, 20-23). The contact angle decreased by 40° using 20 — 25 V actuation voltage in 0.05 s with 100 nm silicon oxide layer as dielectric and 20 nm amorphous fluoropolymer as hydrophobic layer (21). On the EWOD device shown in Table 1, a droplet wets the electrode on the right side where it is attracted by the applied voltage, pulling itself to the right. However, the requirement of high voltages (24) and reliability issues such as electric charging (25, 26) and dielectric breakdown (27, 28) hinder wider adoption and commercialization of EWOD DMF (17, 19).

An alternative to EWOD, surfactant-mediated electro-dewetting (29) has recently been developed. Electro-dewetting-based DMF requires much lower actuation voltages and eliminates the need for dielectric and hydrophobic layers, thereby free of the reliability issues associated with the two layers (30). Mechanistically opposite to electro-wetting, which electrically attracts liquid on a hydrophobic surface, electro-dewetting electrically repels liquid on a hydrophilic surface. The an electric field and adsorbed on the hydrophilic substrate. The hydrophobic tails of the adsorbed surfactants render the surface more hydrophobic, thus increasing the contact angle of droplet (29, 31, 32). A sessile drop test for electro-dewetting was conducted on a bare silicon electrode with native oxide as hydrophilic layer. The droplet used was deionized (DI) water containing 0.015 critical micelle concentration (CMC) of dodecyltrimethylammonium bromide (DTAB). The contact angle increased by 20° using only 3 V actuation voltage in 0.5 s (29). Electro-dewetting exhibits a slower dynamic response, likely due to the time required for the migration and assembly of surfactant molecules, while the polarization of the dielectric layer in EWOD is nearly instantaneous (29). Although the device operates without a top plate in ambient air, which requires consideration of droplet evaporation, several strategies can be employed to mitigate this issue, including oil encapsulation (33), humidity control, and the use of low-volatility liquids.

On the electro-dewetting device shown in Table 1, a droplet dewets the electrode on the left side where the surfactant is absorbed by the applied voltage, pushing itself to the right. The surfactant concentration is commonly effective between 0.015 — 0.1 CMC. When the surfactant concentration is too low, there are insufficient molecules to significantly alter surface wettability. Conversely, if the concentration is too high, the contact angle may already be large before actuation, leaving little room for further increase (29). The very low surfactant concentration used in electro-dewetting minimally affects droplet behavior, and droplet generation, transportation, splitting, and merging were successfully achieved in passive-matrix device (29).

To facilitate complex droplet operations essential for DMF devices, a substantial number of independently accessible electrodes are required, typically arranged in an m × n array on

[a] The Hong Kong University of Science and Technology, Hong Kong. Email: xiexinying@ust.hk; eetlei@ust.hk
[b] University of California, Los Angeles, USA.

View Article Online
DOI: 10.1039/D5LC00992H

ARTICLE

Table 1 Digital microfluidics devices based on EWOD or electro-dewetting and built on direct-drive or AM electrodes. Each of the direct-drive electrodes is connected directly to an independent channel of an external control circuit. Each of the AM electrodes is powered by an own set of transistors.

Liquid actuation mechanism / Electrode addressing scheme	EWOD	Electro-dewetting
Direct-drive 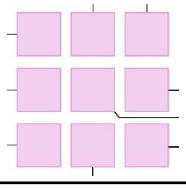	Direct-Drive EWOD DMF (14, 34-38)	Direct-drive electro-dewetting DMF (29, 39)
AM 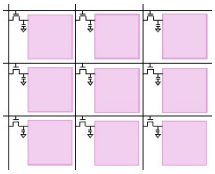	AM EWOD DMF (11, 40-43)	AM electro-dewetting DMF (44), this work

the device substrate as summarized in Table 1. Both EWOD (34-38) and electro-dewetting (29, 39) devices utilize direct-drive control, which involves connecting each of the m × n electrodes (Table 1) to a dedicated external control circuit. However, this direct-drive approach, requiring m × n control lines, can lead to line interference and limit the number of electrodes (45, 46). In the case of EWOD, direct-drive control was introduced to allow m + n control lines to drive the m × n electrodes (47) but presented with limitation. This limitation has been overcome by adopting active-matrix (AM) control based on thin-film transistors (TFT) (41, 43, 48-53) (Table 1). Unfortunately, the single-TFT cell circuit developed for EWOD DMF is not applicable to electro-dewetting DMF because unlike EWOD DMF, which requires a high voltage with no current, electro-dewetting DMF requires a small but continuous current with a low voltage (29, 30). Consequently, most cell circuit configurations for EWOD AM–control (42, 49, 54, 55) are not applicable to electro-dewetting DMF devices.

In this study, an AM electro-dewetting system is designed, constructed and characterized for DMF by deploying a unique cell circuit that supports continuous current. The cell circuits are realized using top-gate (TG) self-aligned (SA) Amorphous metal oxide semiconductor (AMOS) indium-tin-zinc oxide (ITZO) TFTs, as AMOS TFTs have demonstrated superior performance, exhibiting enhanced device uniformity and lower costs compared to low-temperature polycrystalline silicon (LTPS) alternatives (56, 57) and higher mobility than amorphous silicon (a-Si:H) (57). The most widely explored AMOS materials for TFT active layers are indium-gallium-zinc oxide (IGZO) and ITZO. ITZO TFTs exhibits a mobility approximately three times higher than that of IGZO TFTs and the higher mobility of the TFTs would allow a lower V_{DD} to actuate the droplet. Also, ITZO TFTs have already been successfully deployed in a 56-inch OLED TV. This demonstrates their suitability for large-scale production and reinforces their potential for widespread use in active matrix DMF devices (57, 58). Basic DMF operations, including droplet transport, splitting, and merging have been demonstrated at a reduced voltage of 25 V, compared to the >40 V (40, 41, 59) for common AM DMF systems based on EWOD as well as the 32 V used for the preliminary AM IGZO electro-dewetting device (44) that preceded this work.

View Article Online
DOI: 10.1039/D5LC00992H

ARTICLE

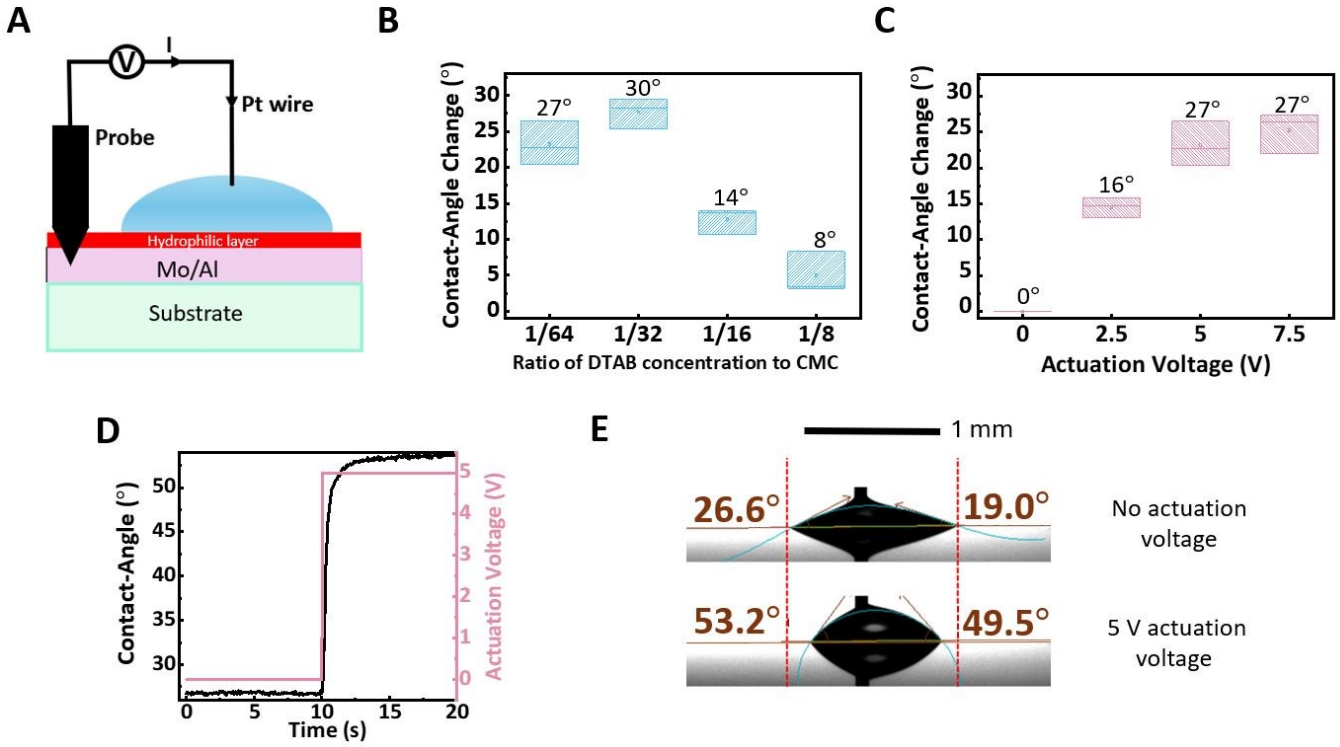

Fig. 1 A) Experiment setup for electro-dewetting sessile droplet test. B) Impact of DTAB concentrations (1/64, 1/32, 1/16, 1/8 CMC) on the change in contact angle induced by electro-dewetting, expressed as a ratio of concentration to critical micelle concentration (CMC). C) Effect of actuation voltage on the electro-dewetting-induced change in contact angle, with applied voltages of 0, 2.5, 5, and 7.5 V, while the electrode remains grounded. D) The response time of electro-dewetting induced contact-angle change with 5 V actuation voltage. E) Contact-angle change of DTAB-laden droplet when 5 V actuation voltage is applied.

Electro-dewetting

The commonly used source/drain (S/D) electrode material for of ITZO TFT is molybdenum (Mo) beneath aluminum (Al) (60, 61). To determine the optimal experiment conditions for electro-dewetting with the above metal electrode and hydrophilic surface material for AM DMF device, a sessile droplet test was used to characterize the contact-angle change induced by electro-dewetting, as schematically illustrated in Fig. 1A. The hydrophilic material applied is 30-nm SiO_x, thin enough to allow for currents, ensuring that it does not obstruct the current flowing through the droplet. A probe was used to contact the metal, while a platinum (Pt) wire with a diameter of 0.1 mm was inserted into the droplet. The contact angle was measured three times using a contact angle meter (Biolin Theta) at different positions under each condition. The effect of ionic surfactant concentration was studied first. Following the original paper of electro-dewetting by Li *et al* (29), cationic surfactant dodecyltrimethylammonium bromide (DTAB) was selected and tested under various concentrations in deionized (DI) water for electro-dewetting. As shown in Fig. 1B, the maximum contact-angle change was ~ 30° at 1/32 CMC under 5 V actuation voltage, while further increase of the DTAB concentration led to a drop of the contact-angle change. These results aligned with the previous findings on bare Si with native oxide (29).

Various voltages were applied between the droplet and the substrate to find the optimal actuation voltage for electro-dewetting. As shown in Fig. 1C, 5 V induced a maximum contact-angle change of ~ 27° with 1/64 CMC DTAB and further increasing the voltage did not lead to a larger contact-angle change. Also, electrolysis and bubble formation were only observed at high voltage of 7.5 V. At 5 V or below, any signs of electrolysis were not observed.

As shown in Fig. 1D, with 1/64 CMC DTAB and 5 V actuation voltage, the droplet exhibited a large contact-angle change (i.e., ~ 27°) and a fast response speed (i.e., < 2 s).

Contact angles and the cross-section views of the droplets in the wetted (without actuation voltage) and dewetted (with 5 V actuation voltage) states are shown in Fig. 1E.

View Article Online
DOI: 10.1039/D5LC00992H

ARTICLE

Cell design for AM electro-dewetting DMF

In conventional 1-TFT-1-capacitor (1T1C) cell configuration (Fig. 2A) to achieve AM control, when a scan pulse is applied to activate the TFT, data is allowed to be transmitted to the S/D terminal and stored on the capacitor (48, 52). However, for electro-dewetting DMF device, which does not have a dielectric layer, a droplet provides a conductive path for electric current to flow through it. Consequently, the capacitor in traditional 1T1C cell circuit is unable to effectively store the charges to maintain a stable electric field for driving surfactant migration in electro-dewetting. See the simulation results with Fig. S1 in Supplementary Information.

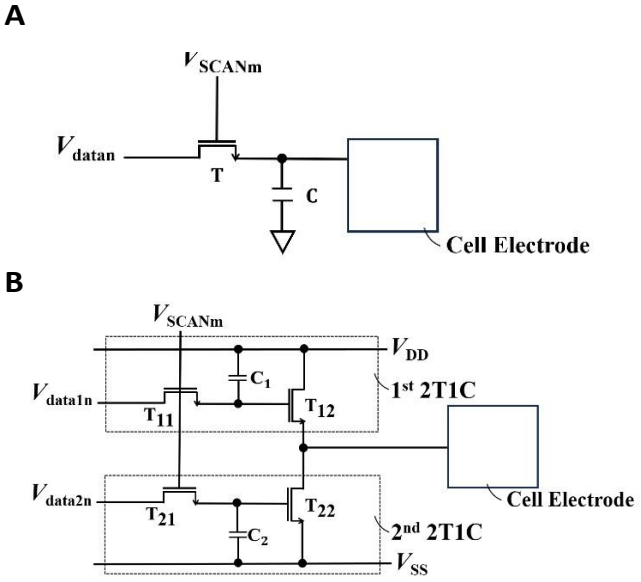

Fig. 2 Schematic cell circuit of A) the conventional 1T1C configuration and B) the designed 4T2C configuration for AM electro-dewetting DMF device.

The designed cell circuit consists of two identical "2-TFTs-1-capacitor (2T1C)" sub-cell circuits, as illustrated in Fig. 2B. The 2T1C circuit includes the addressing TFTs T_{11} or T_{21}, the driving TFTs T_{12} or T_{22}, and the storage capacitors C_1 or C_2, respectively. The gate electrodes of T_{11} and T_{21} are connected to receive the scan signal (V_{SCANm}) for AM addressing. When the V_{SCANm} is "HIGH", the S/D terminals of T_{11} and T_{21} receive the data signals V_{data1n} and V_{data2n}, respectively, which are stored on C_1 and C_2. When V_{data1n} is "HIGH" and V_{data2n} is "LOW", T_{12} is turned on while T_{22} is turned off, and the cell electrode is connected to V_{DD} through T_{12} and placed in the "HIGH" state. Conversely, when V_{data1n} is "LOW" and V_{data2n} is "HIGH", T_{12} is turned off and T_{22} is turned on, and the cell electrode is connected to V_{SS} through T_{22} and placed in the "LOW" state. When V_{data1n} and V_{data2n} are both "LOW", T_{12} and T_{22} are both turned off, resulting in the cell electrode being disconnected from the power lines and placed in the "OPEN" state.

As schematically illustrated in Fig. 3, the electrode in Cell 2 is "HIGH" and connected to V_{DD} through T_{12}, while the electrode in Cell 1 is connected to V_{SS} through T_{22}. A current flows from V_{DD} through T_{12} in Cell 2, the droplet, T_{22} in Cell 1, and finally to V_{SS}. When a positively charged cationic surfactant such as DTAB is used, DTAB molecules will be driven to migrate towards V_{SS} in Cell 1, causing the droplet to move towards the Cell 2.

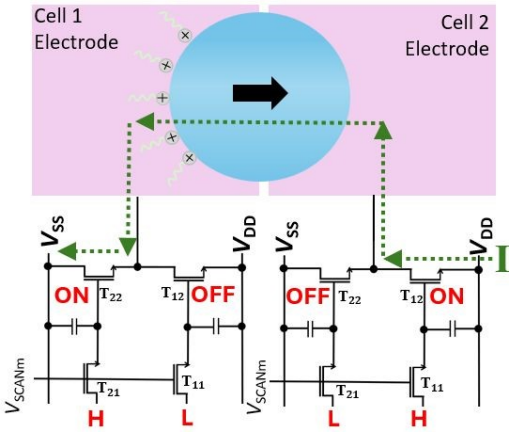

Fig. 3 Working principle of droplet transport in the AM electro-dewetting DMF device. Droplet containing DTAB spans two adjacent cell electrodes.

The driving TFTs T_{12} in Cell 2 and T_{22} in Cell 1 regulate current magnitude. Thus, a lower resistance of the driving TFTs would allow a lower V_{DD} to actuate the droplet. Consequently, higher mobility of the active layer in the TFTs will decrease TFT resistance. Also, the width (W) was increased to 20 µm to decrease TFT resistance. Simultaneously, length (L) of 10 µm was maintained to prevent short-channel effects.

To set the cell electrode state at the (m, n) cell point in the m × n AM, the data signals (V_{data1n} and V_{data2n}) for the n^{th} column are applied to the S/D of addressing transistors when scan pulse V_{SCANm} is "HIGH" to turn on the addressing transistor at the m^{th} row. The data signals (V_{data1n} and V_{data2n}) for the n^{th} column are then stored on the capacitors at the (m, n) cell point. When V_{SCANm} transitions to "LOW", the addressing transistor at the m^{th} row are turned off. The stored data on capacitor which controls the driving transistor, will remain at the desired level until the next time when V_{SCANm} is "HIGH".

The simulation of node potential and the current across the droplet in a 4T2C configuration for a 2×1 AM electro-dewetting application AM operation are illustrated with Fig. S2 in Supplementary Information. This configuration allows the current to be sustained across the droplet during electro-dewetting operation.

View Article Online
DOI: 10.1039/D5LC00992H

ARTICLE

The storage capacitors are 3 pF. As shown with Fig. S3 in Supplementary Information, the discharging time from 20 to 0 V is significantly faster, at ~5 µs, while the charging time to increase from 0 to 20 V is ~47 µs. To ensure adequate charging, the scan signal pulse width was set to 200 µs, which exceeds the minimum required width of 50 µs. The 3-pF capacitor provides ample charge storage capacity, maintaining stable gate voltages for the ITZO driving TFT, with a gate current of approximately 1 pA during operation. The cell circuit configuration allows the capacitor to hold the necessary charge to sustain the gate voltage over time without significant droop. Consequently, the voltage V(V1) at the electrode effectively follows the charging and discharging of V(VC1), ensuring reliable actuation.

To turn off addressing TFTs (i.e., T_{11} and T_{21}), V_{SCANm} should be set low. The V_{gs} for T_{11} and T_{21} given by $V_{\mathrm{gs}} = V_{\mathrm{SCANm}} - V_{\mathrm{data1n}}$ and $V_{\mathrm{gs}} = V_{\mathrm{SCANm}} - V_{\mathrm{data2n}}$, respectively, must be smaller than the turn on voltage (V_{on}) of both T_{11} and T_{21}. V_{on} is defined as the V_{g} needed to generate an $I_{\mathrm{d}} = 10$ pA. For low level of V_{SCANm} set to be 0 V, the low level of V_{data1n} and V_{data2n} are set to be 3.3 V to ensure T_{11} and T_{21} are fully turned off when V_{SCANm} is "LOW". Therefore, the range of V_{SCANm} is 0 V – V_{DD}, while the ranges for V_{data1n} and V_{data2n} are 3.3 V – V_{DD}.

To turn off driving-TFTs T_{12} and T_{22}, the V_{data1n} and V_{data2n} should be "LOW" (3.3 V). The V_{gs} for T_{11} and T_{21} given by $V_{\mathrm{gs}} =$ 3.3 V $- V_{\mathrm{SS}}$ and $V_{\mathrm{gs}} =$ 3.3 V $- V_{\mathrm{SS}}$ of T_{22}, respectively, must also be smaller than the V_{on} of T_{12} and T_{22}. Consequently, V_{SS} is set to be 8 V to ensure that both T_{12} and T_{22} can be fully turned off.

Fabrication of AM electro-dewetting DMF device

As shown in Fig. 4, the fabrication process began with the sputtering and patterning of 150 nm molybdenum (Mo) layer on oxidized Si substrate as the data lines for inputting V_{data1n} and V_{data2n} as well as one electrode of the storage capacitor (CE1). 50-nm SiN_y dielectric was subsequently deposited. Next, 100-nm SiO_x was deposited. This SiO_x/SiN_y stack serves as the 1st interlayer dielectric layer (ILD1) (Fig. 4A). Then, 25-nm ITZO was deposited and patterned as active layer for both TFTs in the 2T1C-circuit and the second electrode of the storage capacitor (CE2). The 100-nm SiO_x layer was then formed as the gate insulator (GI). A "post-GI" furnace anneal was performed in O_2 to oxidize the active layer and eliminate defects at the interface between the GI and the active layer (Fig. 4B). Following this,

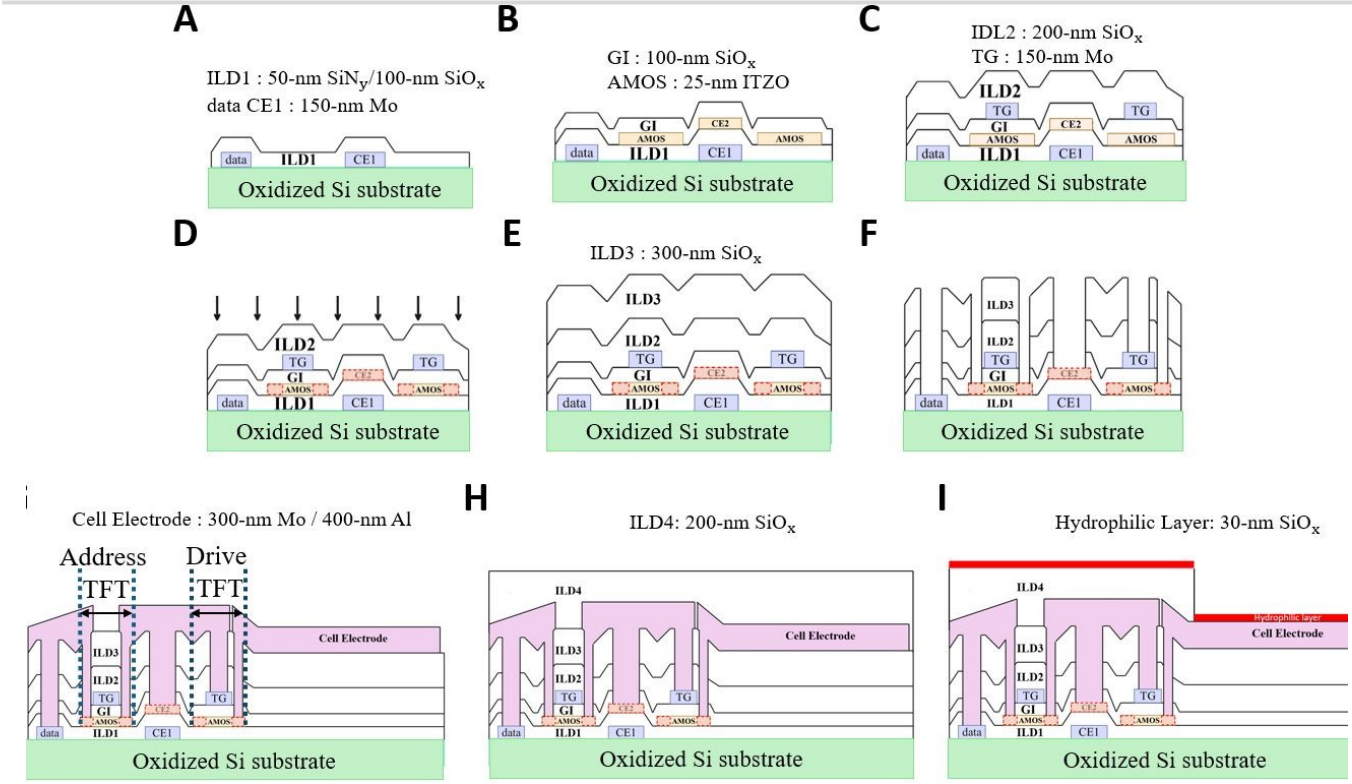

Fig. 4 Microfabrication process of the electro-dewetting DMF device integrated with AM of TG SA TFT ITZO: A) sputtering and patterning of Mo as data lines and CE1, followed by deposition of ILD1; B) deposition and patterning of active layer for both TFTs in the 2T1C-circuit and CE2, followed by deposition of GI; C) sputtering and patterning of Mo as TG, followed by deposition of ILD2; D) S/D activation; E) deposition of ILD2; F) opening of contact hole; G) sputtering and patterning of Mo/Ti stack to form the connection, and cell electrode; H) deposition of ILD4; I) exposure of the cell electrode, followed by deposition of hydrophilic layer.

150-nm Mo was sputtered and patterned to serve as the TG of the TFTs, and the scan line for inputting V_{SCANm}. The 200-nm SiO_x layer as the 2nd interlayer dielectric layer (ILD2) was subsequently deposited (Fig. 4C), followed by annealing at in O_2. SA S/D regions of the TFTs were then formed (Fig. 4D). The 300-nm SiO_x was subsequently deposited using PECVD, as the 3rd interlayer dielectric layer (ILD3) to repair the damage from SA S/D formation (Fig. 4E). Contact holes were then opened (Fig. 4F). Next, stacks of 300-nm Mo beneath 400-nm titanium (Ti) were sputtered and patterned to form the connections, and the cell electrode (Fig. 4G). Ti was used as it offers superior stability during the electro-dewetting process, whereas other conductive materials that are more chemically active, such as aluminum (Al), can be damaged under similar conditions. 200-nm SiO_x was then deposited as the 4th interlayer dielectric layer (ILD4) isolating the Mo/Ti connection lines from the droplet (Fig. 4H). The cell electrodes were then exposed. Finally, hydrophilic layer was deposited using 30-nm SiO_x (Fig. 4I), thin enough for current flowing through the droplet and compatible with the TFT fabrication process.

The 8×8 AM arrays have been constructed based on the above fabrication process, as illustrated in Fig. 5A. The arrays feature cell size of 2 mm × 2 mm (Fig. 5B) with the cell circuits shown in Fig. 5C.

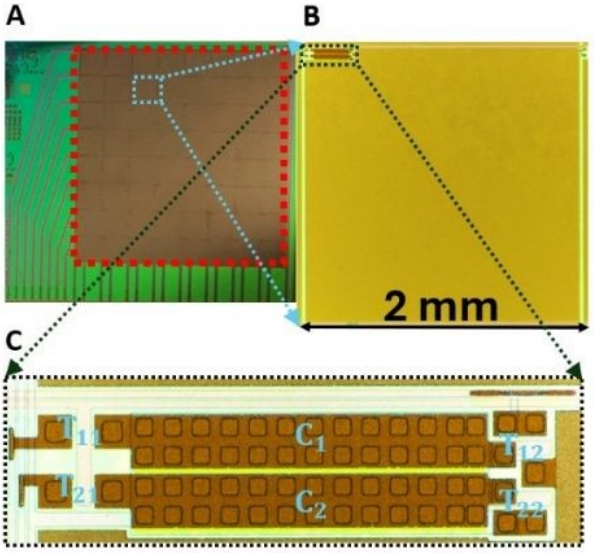

Fig. 5 Pictures of A) 8×8 AM array for electro-dewetting, B) its cell and C) its cell circuit

ITZO TFTs Performance

To evaluate the stability of ITZO TFTs under current stress, the device was subjected with $V_{\mathrm{gs}} =$ 15 V and $V_{\mathrm{ds}} =$ 5 V to simulate ITZO TFT under electro-dewetting operation. The evolution of the transfer characteristics is shown in Fig. 6. Notably, the ITZO TFTs maintained consistent performance even after 1000 s of current stress.

The I_{d} vs. V_{g} transfer characteristics at $\mathrm{V_d} =$ 0.5 V and 5 V of TG SA ITZO TFTs with *W/L* = 10 / 10 μm (addressing TFTs) and *W/L* = 20 / 10 μm (driving TFTs) were measured at 15 different positions across a 4-inch wafer, as presented in Fig. 7. The position numbers on the wafer are shown in the inset of the transfer characteristics. The performance of the TFTs are largely uniform across the wafer.

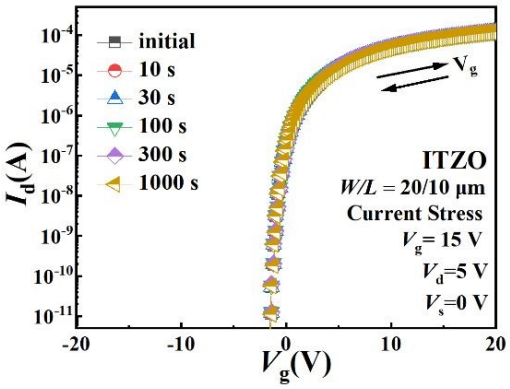

Fig. 6 The evolution of I_{d} *vs.* V_{g} transfer characteristics with current stress time

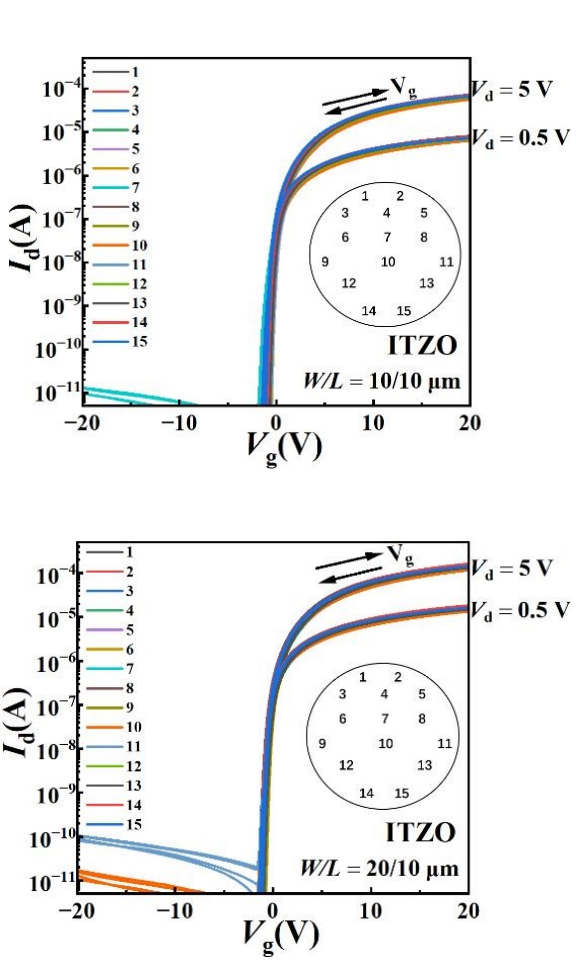

Fig. 7 The transfer characteristics of TFTs of A) *W/L* = 10 / 10 μm and B) *W/L* = 20 / 10 μm at different positions of the wafer. The position numbers on the wafer are shown in the insets.

The ITZO TFTs with above fabrication process exhibit good repeatability across the past four years (62-65). The electronic

View Article Online
DOI: 10.1039/D5LC00992H

parameters of ITZO TFTs with $W/L = 10/10$ µm and $10/20$ µm are summarized in Table 2, extracted from TFTs respectively at a low $V_{\mathrm{d}} = 0.5$ V. The field-effect mobility $\mu_{\mathrm{FE}} \equiv Lg_{\mathrm{m}}/(WC_{\mathrm{i}}V_{\mathrm{d}})$, where g_{m} is the maximum trans-conductance and C_{i} is the gate capacitance per unit area. The sub-threshold slope (SS) is extracted from the minimum value of $\partial \log I_{\mathrm{d}}/\partial V_{\mathrm{g}}$ for $V_{\mathrm{g}} > V_{\mathrm{on}}$.

Table 2: The electronic parameters of ITZO TFTs with $W/L =$ 10/10 µm and 10/20 µm

W/L (µm)	μ_{FE} (cm²/Vs)	SS (mV/dec)	V_{on} (V) ($V_{\mathrm{g}}@I_{\mathrm{d}} = 1$ pA)	I_{off} (A)
0/10	~ 40	~225	−0.16 ~ −0.8	$< 10^{-11}$
20/10	~ 40	~200	−0.14 ~ −0.8	$< 10^{-10}$

Experiments for DMF operation and discussion

To assess droplet manipulation capability of the developed AM electro-dewetting DMF device, a series of experiments for basic DMF operations was performed. As schematically illustrated in Fig. 8, the experiment setup included: a computer that runs a LabView program as the graphical user interface; a microcontroller; a driver board powered by a DC voltage supply; and the AM electro-dewetting chip connected with the driver circuit through a flexible printed circuit (FPC).

The cell electrode states ("HIGH," "LOW," or "OPEN") within the array are set using LabVIEW, which packs the corresponding V_{data1n} and V_{data2n} for each cell and sends the data pack to the microcontroller (STM32F407ZG). The microcontroller controls HV66 on the driver board, a low-voltage serial to high-voltage parallel converter, to output V_{SCANm} ranging from 0 V to V_{DD}. This is achieved by generating Data, Clock (CLK), Latch Enable (LE) and Blank (BL) signals (0 V — 3.3 V) for the HV66. The microcontroller controls another HV66 to output V_{data1n} and V_{data2n} from 3.3 V to V_{DD} by using adder circuit to raise the input signals (0 V — 3.3 V) from microcontroller to a range spanning from 3.3 V to 6.6 V.

Basic DMF droplet operations for the AM electro-dewetting device such as transporting, splitting, and merging, have been demonstrated, as highlighted in Fig. 9. As shown in Fig. 9A, a DI water droplet containing 1/64 CMC DTAB, with its pH adjusted to 4.5 to alleviate "autophobing" (66, 67), was placed on the AM electro-dewetting device. As shown in Fig. 9B, the rear end of the droplet was repelled to retract. Note that since a cationic surfactant was used, any electrode actuated as "LOW" will attract those surfactant molecules and repel the droplet. To drive the droplet to move along a desired pathway, we applied "LOW" voltage to the electrodes surrounding the droplet pathway, which constantly repels and confines the droplet during transporting. As shown from Figs. 9B to 9F, all electrodes in front of the droplet were constantly actuated to be "HIGH" during the transporting process. That was to ensure that those electrodes in front of the droplet never repels it regardless of how many electrodes the droplet spans across during movement. This extra caution was taken since the inactivated electrode can connect to the activated electrodes through the droplet, which may disrupt the intended transport path to move forward depending on the droplet shape. This interaction can lead to unintended repulsion or attraction forces that affect the droplet movement. To mitigate this issue, it is essential to maintain a stable voltage on the electrodes. By applying a "HIGH" on the electrodes in the intended transport path, the droplet path can be well controlled. Satellite droplets are observed during transportation in Figs. 9E, 9F, and 9L. This can indeed introduce contamination and present challenges during droplet transportation. One effective approach to address this issue is to enhance the surface smoothness of the electrodes. Currently, the droplet must "climb" over the "hill" formed by the ILD4 layer situated between adjacent cell electrodes as shown in Fig. 4I. Potential mitigation strategy is to improve the fabrication process to enhance the flatness of the surface. For example, cell

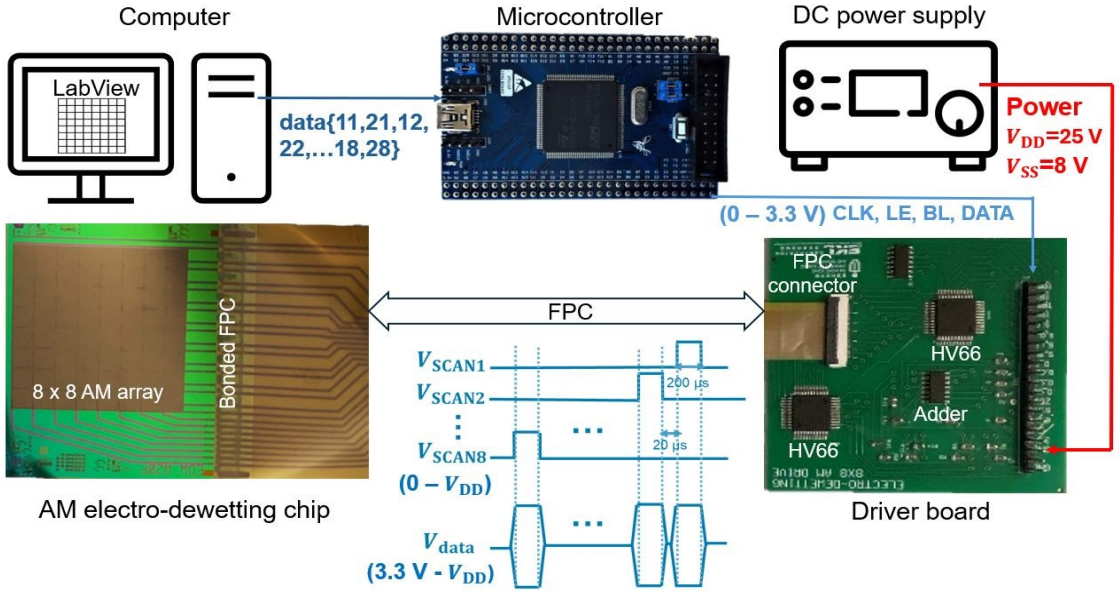

Fig. 8 Experiment setup to control the AM electro-dewetting chip for DMF operations

View Article Online
DOI: 10.1039/D5LC00992H

ARTICLE

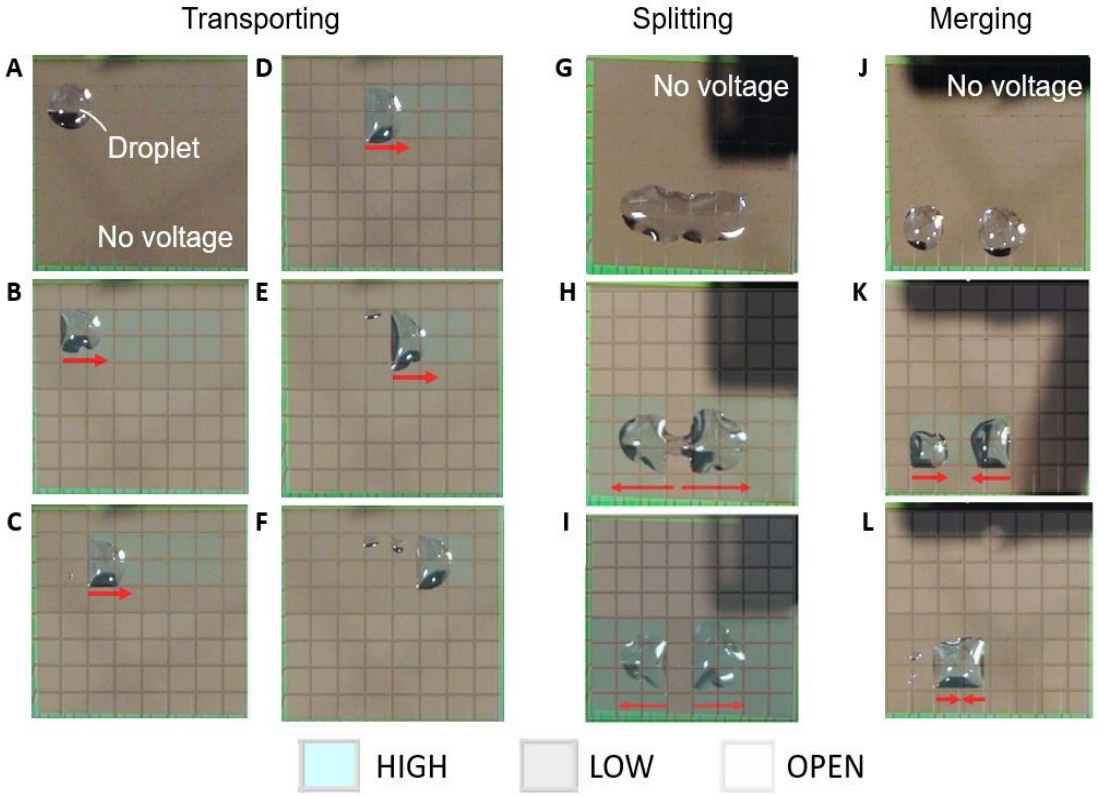

Fig. 9 Basic droplet operations and corresponding actuation scheme. The actuation state for each electrode is indicated by colour, i.e., blue for "HIGH", grey for "LOW", and white for "OPEN". The schematic pictures of actuation schemes for the 8 x 8 array are made transparent and are overlaid with pictures of droplet operations to indicate the actuation states for each step and each electrode during the droplet operation process. A–F) Droplet pictures and corresponding actuation scheme for droplet transport. G-I) Droplet pictures and corresponding actuation scheme for droplet splitting. J-L) Droplet pictures and corresponding actuation for droplet merging.

electrodes may be deposited after ILD4 layer to reduce the "hill". The average speed of transportation is 0.15 mm/s.

As shown in Figs. 9G to 9I, droplet splitting was demonstrated on the electro-dewetting DMF device. Distinct from the droplet actuation scheme for transporting, the actuation scheme for droplet splitting does not need to confine the droplet since it is desirable to let the left and right edges of the droplet spread in various directions during splitting. Therefore, only a column of electrodes was actuated to be "LOW" so that liquid on these electrodes was repelled to retract, and eventually pinched off, as shown in Fig.9H and 9I. The time taken to split the droplet into two droplets separated by 2 mm was about 6 seconds.

Droplet merging was also demonstrated by using a similar actuation scheme as that for droplet transport, as shown in Figs. 9J to 9K. Merging of two droplets initially separated by 4 mm took around 15 seconds.

The cell-level specifications are summarized in Table 3.

Compared in Table 4 are the AM DMF device in this work and other AM DMF devices in the literature. Compared to the AM EWOD device, the speed of AM electro-dewetting device is slower. However, the lower actuation voltage required for electro-dewetting allowed for reduced voltage of both data and scan signals. Furthermore, the higher mobility of ITZO TFTs (~ 37 cm^2/Vs (68)) compared to indium-gallium-zinc oxide (IGZO) TFTs (~ 16.6 cm^2/Vs (69)) further enabled lower voltage signals compared to our previous work. It is worth noting that despite the very low concentration (i.e., < 1/10 CMC), the reliance on ionic surfactant of electro-dewetting may pose challenges for specific bioassays involving living cells. For biochemical applications, further characterization is necessary to assess the compatibility of the ionic surfactant with the reagents used.

View Article Online
DOI: 10.1039/D5LC00992H

ARTICLE

Table. 3 Cell-level specifications.

Cell Size (mm²)	V_{DD} (V)	V_{SS} (V)	Addressing TFTs (W/L)	Driving TFTs (W/L)
2 × 2	25	8	10/10 μm	20/10 μm

Table. 4 Comparison of the AM DMF device.

	DMF device	Active layer	Cell Circuit	V_{SCAN}(V)	V_{data} (V)	Droplet speed (mm/s)
This work	Electro-dewetting	ITZO	4T2C	0 — 25	3.3 — 25	0.15
(44)	Electro-dewetting	IGZO	4T2C	0 — 32	3.3 — 32	0.04
(1)	EWOD	Not known	1T1C	0 — 50	0 — 40	Not known
(11)	EWOD	IGZO	1T1C	0 — 35	0 — 31	6
(48)	EWOD	a-Si	1T1C	0 — 45	0 — 35	5
(50)	EWOD	a-Si	3T1C	0 — 40	0 — 35	Not known
(55)	EWOD	IGZO	5T1C	0 — 45	0 — 40	Not known

Conclusion

An AM electro-dewetting DMF device with 8 x 8 AM array has been designed, fabricated, and demonstrated for basic droplet operations, addressing the limitations posed by direct-drive control for DMF. By utilizing a "4T2C" cell circuit, continuous current was achieved to drive droplets by the mechanism of surfactant-mediated electro-dewetting. The maximum voltage required for the AM electro-dewetting device is only 25 V, which is lower than that of typical AM EWOD DMF devices. By eliminating the need for dielectric and hydrophobic layers, the AM electro-dewetting device paves the way for more reliable AM DMF systems, making it suitable for a diverse range of lab-on-a-chip applications. While the proof-of-concept device for active-matrix electro-dewetting has been demonstrated, system-level performances such as device lifetime, droplet volume consistency, and parallel multi-droplet operation have not been extensively characterized. It is acknowledged that further investigation will be conducted to address these limitations.

Author contributions

C.-J.K. and M.W. conceived and initiated the research; X.X. designed the layout, developed the fabrication process, fabricated the device, wrote the code for microcontroller, programmed LabView, designed PCB board and conducted the experiment; X.X, Q.L.W. and R.S. discussed the experiment and fabrication process. X.X., R.S., T.L. and M.W. discussed the cell circuit; M.W., Q.L.W. and C.-J.K. revised the manuscript. M.W. supervised the research. All authors discussed the results and commented on the manuscript.

Conflicts of interest

The authors declare no conflict of interest.

Acknowledgements

The devices were fabricated at The Nanosystem Fabrication Facility (NFF) of The Hong Kong University of Science and Technology. Q.L.W. and C.-J.K. were partially supported by the National Science Foundation (1711708).

References

1.Hu S, Ye J, Shi S, Yang C, Jin K, Hu C, et al. Large-area electronics-enabled high-resolution digital microfluidics for parallel single-cell manipulation. Analytical Chemistry. 2023;95(17):6905-14.
2.Streets AM, Huang Y. Chip in a lab: Microfluidics for next generation life science research. Biomicrofluidics. 2013;7(1).
3.Wu J, Fang H, Zhang J, Yan S. Modular microfluidics for life sciences. Journal of Nanobiotechnology. 2023;21(1):85.
4.Jiang K, Dong C, Xu Y, Wang L. Microfluidic-based biomimetic models for life science research. RSC Advances. 2016;6(32):26863-73.
5.Adam T, Hashim U, Foo K. Microfluidics design and fabrication for life sciences application. Advanced Science Letters. 2013;19(1):48-53.
6.Xiong B, Ren K, Shu Y, Chen Y, Shen B, Wu H. Recent developments in microfluidics for cell studies. Advanced materials. 2014;26(31):5525-32.
7.Xing Y, Liu Y, Chen R, Li Y, Zhang C, Jiang Y, et al. A robust and scalable active-matrix driven digital microfluidic platform based on printed-circuit board technology. Lab on a Chip. 2021;21(10):1886-96.

8. Van Nguyen H, Kim KY, Nam H, Lee SY, Yu T, Seo TS. Centrifugal microfluidic device for the high-throughput synthesis of Pd@ AuPt core-shell nanoparticles to evaluate the performance of hydrogen peroxide generation. Lab on a Chip. 2020;20(18):3293-301.
9. Breslauer DN, Lee PJ, Lee LP. Microfluidics-based systems biology. Molecular Biosystems. 2006;2(2):97-112.
10. Dressler OJ, Casadevall i Solvas X, DeMello AJ. Chemical and biological dynamics using droplet-based microfluidics. Annual Review of Analytical Chemistry. 2017;10:1-24.
11. Noh JH, Noh J, Kreit E, Heikenfeld J, Rack PD. Toward active-matrix lab-on-a-chip: programmable electrofluidic control enabled by arrayed oxide thin film transistors. Lab on a Chip. 2012;12(2):353-60.
12. Pinho B, Girardon S, Bazer-Bachi F, Bergeot G, Marre S, Aymonier C. A microfluidic approach for investigating multicomponent system thermodynamics at high pressures and temperatures. Lab on a Chip. 2014;14(19):3843-9.
13. Sevim S, Sorrenti A, Franco C, Furukawa S, Pané S, deMello AJ, et al. Self-assembled materials and supramolecular chemistry within microfluidic environments: from common thermodynamic states to non-equilibrium structures. Chemical Society Reviews. 2018;47(11):3788-803.
14. Cho SK, Moon H, Kim C-J. Creating, transporting, cutting, and merging liquid droplets by electrowetting-based actuation for digital microfluidic circuits. Journal of Microelectromechanical systems. 2003;12(1):70-80.
15. Choi K, Ng AH, Fobel R, Wheeler AR. Digital microfluidics. Annual review of analytical chemistry. 2012;5(1):413-40.
16. Xu Y, Wu W, Zhou Z, Su Q, Liu X, Li W, et al. Digital Microfluidic Lab-on-a-Chip on a TFT Glass Substrate Enabling Point-of-Care Testing. IEEE Electron Device Letters. 2023.
17. Li J, Kim C-J. Current commercialization status of electrowetting-on-dielectric (EWOD) digital microfluidics. Lab on a Chip. 2020;20(10):1705-12.
18. Lee J, Moon H, Fowler J, Schoellhammer T, Kim C-J. Electrowetting and electrowetting-on-dielectric for microscale liquid handling. Sensors and actuators A: Physical. 2002;95(2-3):259-68.
19. Wang QL, Cho EH, Li J, Huang HC, Kin S, Piao Y, et al. Democratizing digital microfluidics by a cloud-based design and manufacturing platform. Lab on a Chip. 2024;24(19):4536-48.
20. Ren H, Fair RB, Pollack MG. Automated on-chip droplet dispensing with volume control by electro-wetting actuation and capacitance metering. Sensors Actuators B: Chemical. 2004;98(2-3):319-27.
21. Moon H, Cho SK, Garrell RL, Kim C-J. Low voltage electrowetting-on-dielectric. Journal of applied physics. 2002;92(7):4080-7.
22. Mugele F, Buehrle J. Equilibrium drop surface profiles in electric fields. Journal of Physics: Condensed Matter. 2007;19(37):375112.
23. Nelson WC, Kim C-J. Droplet actuation by electrowetting-on-dielectric (EWOD): A review. Journal of Adhesion Science Technology. 2012;26(12-17):1747-71.
24. Wang QL, Li J, Cho HSE, Xu L, Wang A, Kuiry S, et al. A Versatile Control System for Digital Microfluidic Chips of Varying Types, Shapes, Sizes, and Thicknesses. International Conference on Micro Electro Mechanical Systems (MEMS); 2024. p. 1138-41.
25. Thomas D, Audry MC, Thibaut RM, Kleimann P, Chassagneux F, Maillard M, et al. Charge injection in dielectric films during electrowetting actuation under direct current voltage. Thin Solid Films. 2015;590:224-9.
26. Koo B, Kim C-J. Evaluation of repeated electrowetting on three different fluoropolymer top coatings. Journal of Micromechanics Microengineering. 2013;23(6):067002.
27. Raj B, Dhindsa M, Smith NR, Laughlin R, Heikenfeld J. Ion and liquid dependent dielectric failure in electrowetting systems. Langmuir. 2009;25(20):12387-92.
28. Huang LX, Koo B, Kim C-J. Sputtered–Anodized Ta2O3 as the Dielectric Layer for Electrowetting-on-Dielectric. Journal of Microelectromechanical systems. 2013;22(2):253-5.
29. Li J, Ha NS, Liu T, van Dam RM, Kim C-J. Ionic-surfactant-mediated electro-dewetting for digital microfluidics. Nature. 2019;572(7770):507-10.
30. Wang QL, Kim C-J. An Electro-Dewetting Based Microfluidic Pixel Device. International Conference on Micro Electro Mechanical Systems (MEMS); 2025. p. 1245-8.
31. Chu W, Ji H, Wang QL, Kim C-J, Bertozzi AL. Electrohydrodynamics modeling of droplet actuation on a solid surface by surfactant-mediated electrodewetting. Physical Review Fluids. 2023;8(7):073701.
32. Wang QL, Tian P, Kim C-J. Surfactant-mediated electro-dewetting of droplets in oil for liquid-shape manipulation. Droplet. 2025;4:e70033.
33. Jebrail MJ, Renzi RF, Sinha A, Van De Vreugde J, Gondhalekar C, Ambriz C, et al. A solvent replenishment solution for managing evaporation of biochemical reactions in air-matrix digital microfluidics devices. Lab on a Chip. 2015;15(1):151-8.
34. Pollack MG, Shenderov AD, Fair RB. Electrowetting-based actuation of droplets for integrated microfluidics. Lab on a Chip. 2002;2(2):96-101.
35. Gong J, Kim C-J. Direct-referencing two-dimensional-array digital microfluidics using multilayer printed circuit board. Journal of microelectromechanical systems. 2008;17(2):257-64.
36. Zhang K, Wang W, Li C, Riaud A, Zhou J. 2D large-scale EWOD devices with honeycomb electrodes for multiplexed multidirectional driving of micro-droplets. AIP Advances. 2020;10(5).
37. Ko H, Lee J, Kim Y, Lee B, Jung CH, Choi JH, et al. Active digital microfluidic paper chips with inkjet-printed patterned electrodes. Adv Mater. 2014;26(15):2335-40.
38. Naorungroj S, Kin S, Chun S, Lee SH, Kwon OS, Wang QL, et al. High-sensitivity electrochemical detection of HPV DNA via enzyme-amplified target-induced hairpin opening on a thermally controlled paper-based digital microfluidic platform. Biosensors and Bioelectronics. 2025:117898.
39. Li J, Kim C-J. Electrodewetting on transparent substrate: device fabrication and demonstration. International Conference on Micro Electro Mechanical Systems (MEMS); 2019. p. 180-1.
40. Kalsi S, Sellars SL, Turner C, Sutton JM, Morgan H. A programmable digital microfluidic assay for the simultaneous detection of multiple anti-microbial resistance genes. Micromachines. 2017;8(4):111.
41. Anderson S, Hadwen B, Brown C. Thin-film-transistor digital microfluidics for high value in vitro diagnostics at the point of need. Lab on a Chip. 2021;21(5):962-75.
42. Wang D, Jin K, Ji J, Hu C, Du M, Belgaid Y, et al. Active-matrix digital microfluidics design for field programmable high-throughput digitalized liquid handling. iScience. 2024;27(5).
43. Jia Z, Jiang C, Li J, Belgaid Y, Ge M, Li L, et al. Intelligent single-cell manipulation: LLMs-and object detection-enhanced active-matrix digital microfluidics. Microsystems & Nanoengineering. 2025;11(1):133.
44. Xie X, Wang QL, Hu Y, Shi R, Lei T, Kim C-J, et al. An Active Matrix Electro-dewetting Array for Digital Microfluidics. International Conference on Solid-State Sensors, Actuators and Microsystems (Transducers); Florida, USA. 2025. p. 389-92.

45.Huang HC, Liang CC, Wang QL, Huang X, Ho TY, Kim C-J. Nr-router: Non-regular electrode routing with optimal pin selection for electrowetting-on-dielectric chips. Asia and South Pacific Design Automation Conference (ASP-DAC); 2022. p. 56-61.
46.Pan Y, Liu G, Huang X, Li Z, Huang HC, Liang CC, et al. NR-Router+: Enhanced Non-Regular Electrode Routing With Optimal Pin Selection for Electrowetting-on-Dielectric Chips. Transactions on Computer-Aided Design of Integrated Circuits. 2024;43(9):2606-19.
47.Fan SK, Hashi C, Kim C-J. Manipulation of multiple droplets on N/spl times/M grid by cross-reference EWOD driving scheme and pressure-contact packaging. International Conference on Micro Electro Mechanical Systems, 2003 MEMS-03 Kyoto IEEE; 2003. p. 694-7.
48.Ma H, Shi S, Jin K, Wang D, Hu S, Su Y, et al. Large-area manufacturable active matrix digital microfluidics platform for high-throughput biosample handling. International Electron Devices Meeting (IEDM); 2020. p. 35.5. 1-.5. 4.
49.Hadwen B, Broder G, Morganti D, Jacobs A, Brown C, Hector J, et al. Programmable large area digital microfluidic array with integrated droplet sensing for bioassays. Lab on a Chip. 2012;12(18):3305-13.
50.Yu J, Jiang S, Wang D, Chang C, Jia Z, Du M, et al. Field programmable digital microfluidics chip for high-throughput droplet array manipulation. International Electron Devices Meeting (IEDM); 2023. p. 1-4.
51.Kalsi S, Valiadi M, Tsaloglou MN, Parry-Jones L, Jacobs A, Watson R, et al. Rapid and sensitive detection of antibiotic resistance on a programmable digital microfluidic platform. Lab on a Chip. 2015;15(14):3065-75.
52.Geng D, Wang K, Li L, Myny K, Nathan A, Jang J, et al. Thin-film transistors for large-area electronics. Nature Electronics. 2023;6(12):963-72.
53.Sterling JD, Chen CY. Keck Graduate Institute of Applied Life Sciences. Method, apparatus and article for microfluidic control via electrowetting, for chemical, biochemical and biological assays and the like. US 7,163,612 B2. 2007- 1-16.
54.Jiang S, Wang D, Ma H, Nathan A, Yu J. Low temperature polysilicon pixel circuits for active-matrix digital microfluidic chips. Displays. 2025;88:103048.
55.Zhan S, Liu R, Luo Q, Li Y, Li Y, Liu Z, et al. Implementing AC Signal Driving in Digital Microfluidic Chips with Active-Matrix Thin-Film Transistors. IEEE Sensors Journal. 2024.
56.Lu L, Xia Z, Li J, Feng Z, Wang S, Kwok HS, et al. A comparative study on fluorination and oxidation of indium-gallium-zinc oxide thin-film transistors. IEEE Electron Device Letters. 2017;39(2):196-9.
57.Hosono H, Kumomi H. Amorphous oxide semiconductors: IGZO and related materials for display and memory: John Wiley & Sons; 2022.
58.Shih TH, Ting HC, Chen CL, Tsai L, Chen CY, Lin LF, et al. High mobility metal oxide thin film transistors active-matrix organic light-emitting diode television. International Workshop on Active-Matrix Flatpanel Displays and Devices (AM-FPD); 2014. p. 17-20.
59.Yang Z, Jin K, Chen Y, Liu Q, Chen H, Hu S, et al. AM-DMF-SCP: integrated single-cell proteomics analysis on an active matrix digital microfluidic chip. JACS Au. 2024;4(5):1811-23.
60.Hu Y, Lei T, Jiang W, Zhang Z, Xu Z, Wong M. Spiking Neural Network Based on Memory Capacitors and Metal-Oxide Thin-Film Transistors. IEEE Transactions on Circuits Systems II: Express Briefs. 2024.
61.Hu Y, Ho TSP, Lei T, Xia Z, Wong M. Construction and Application of a Neuromorphic Circuit With Excitatory and Inhibitory Post-Synaptic Conduction Channels Implemented Using Dual-Gate Thin-Film Transistors. IEEE Transactions on Circuits Systems I: Regular Papers. 2024.
62.Xie X, Wong M. The Effects of Oxides Deposited Using Different Precursors on the Characteristics of Top-Gate Indium-Tin-Zinc Oxide Thin-Film Transistors with Self-Aligned, Oxygen-Plasma Activated Source/Drain Regions. International Conference on Display Technology; Xiamen, China. 2025.
63.Lei T, Hu Y, Xie X, Shi R, Wong M. In-Sensor Computing-Based Smart Sensing Architecture Implemented Using a Dual-Gate Meta-Oxide Thin-Film Transistor Technology. Advanced Electronic Materials. 2024:2400572.
64.Lei T, Hu Y, Xie X, Wong M, An active-matrix piezoelectric tactile sensor array with in-pixel amplifier and non-uniformity compensation. 2023 22nd International Conference on Solid-State Sensors, Actuators and Microsystems (Transducers); 2023: IEEE.
65.Xie X, Chen K, Zhou Z, Jiang W, Wang Y, Wang S, et al., P1.4: Oxygen-Plasma Induced Generation of Mobile Charge Carriers in Indium-Tin-Zinc Oxide. SID Symposium Digest of Technical Papers; 2023: Wiley Online Library.
66.Hare E, Zisman W. Autophobic liquids and the properties of their adsorbed films. The Journal of Physical Chemistry B. 1955;59(4):335-40.
67.Bera B, Duits MHG, Stuart MAC, Van Den Ende D, Mugele F. Surfactant induced autophobing. Soft Matter. 2016;12(20):4562-71.
68.Xie X, Chen K, Zhou Z, Jiang W, Wang Y, Wang S, et al., Conductive Indium-Tin-Zinc Oxide Formed Using an Oxygen Plasma Treatment Through a Silicon Oxide Cover Layer. SID Symposium Digest of Technical Papers; 2023: Wiley Online Library.
69.Li J, Zhang Y, Fu H, Yang H, Guan Y, Zhang Y, et al. Self-Aligned Top-Gate Amorphous In-Ga-Zn-O Thin-Film Transistors with Hafnium-Induced Source/Drain Regions. SID Symposium Digest of Technical Papers: Wiley Online Library; 2023. p. 580-2.

View Article Online
DOI: 10.1039/D5LC00992H

- The data supporting this article have been included as part of the Supplementary Information.
- The program for LabVIEW can be found at GUI.vi with LabVIEW. The version of the code employed for this study is LabVIEW 2018.
- The code for microcontroller (STM32F407ZG) can be found at Basic_32x32_regular_Labview. The version of the code employed for this study is MDK 5.